Contents

Chapter 1

Introduction

Since the beginning of the present century there are well known materials which emit a flash of light while the charged particles interact with them. This process is called scintillation.

The scintillators are widely used in particle and nuclear physics. The real career of the scintillation detectors started after the invention of the photomultipliers. Those allowed to replace in an observation a human eye by the electronic and now the weak scintillation signal could be counted with efficiency and reliability compared to that of gaseous ionization detectors. There are a few reasons for the popularity of the scintillation detectors, as for instance their sensitivity to energy (most scintillators give almost linear signal with respect to the deposited energy), their fast time response, and pulse shape discrimination (some of the scintillation detectors can distinguish between different types of particles by analyzing the shape of the emitted pulses). This work considers only the organic scintillator detectors, which are used in COSY-11 experimental setup.

1.1 COSY-11 installation

The production of mesons with and without strangeness in a mass range from the π^o to the $\Phi(1020)$ meson offers a broad field of research in medium energy physics.

COSY-11 [4] was built for studies in this field, especially in the 1 GeV/c^2 meson mass region. The main topics here, are the investigation of different resonances whose structure is still an open question, one of the interesting case is a production of the meson $\eta^{'}$ which also is under discussion concerning the possible gluonium content. The proton cooler synchrotron COSY Jülich provides access to high precision studies with proton momenta up to $\sim$3.4 GeV/c covering a mass range up to 1.018 GeV/c^2.

The COSY-11 installation is an internal experiment at the cooler synchrotron and storage ring COSY Jülich, installed early in 1995. It was designed for full geometrical acceptance close to the threshold for meson production studies, especially in the 1 GeV/c^2 mass range. The experimental setup makes use of a regular C-type COSY dipole magnet to separate reaction products from the beam and to analyze their momenta, thus allowing the observation of charged reaction products at small angles with beam energies close to threshold. Particles are identified by missing mass reconstructions from measured four-momenta of the two outgoing protons in the predominantly studied pp $\rightarrow$ ppX reaction. As target a hydrogen cluster target is installed $\sim$ $30cm$ in the front of the dipole. In Fig.1.1 a sketch of the COSY-11 setup is shown.

The tracks of negatively charged mesons bent towards the inside of the dipole gap are detected by an array of silicon pad detectors (6×25 cm^2) and an additional scintillation counter (6×100 cm^2), both mounted inside the gap.

Positively charged reaction products are, due to their small momenta, separated from the circulating beam by the magnetic field and diverted towards the center of the storage ring. Passing through a specially developed large exit foil (two layers of C-foil 150 μm on 30 μm Al) of the vacuum chamber, which is mounted inside the dipole gap ($\sim$60 mm free height for particle) the ejectiles reach the detection system operating in normal atmosphere.

Two stacks of six and eight drift chamber planes, respectively, (marked as D1 and D2 on fig.1.1) spaced by a distance $\sim$ 80 cm are used to measure the direction of positively charged particles. Thus, a determination of the particles' momentum is possible, by means of the knowledge of the magnetic field. The position resolution in the drift chambers is 250 μm (500 μm) in horizontal (vertical) direction.

Behind the drift chambers are two scintillation hodoscopes, S1 and S2. These consist of sixteen scintillation modules with dimensions of $450\times100\times4$ mm^3 and $450\times13.5\times2$ mm^3, respectively. The scintillator elements are arranged vertically and are read out at both sides by photomultipliers. For minimum ionizing particles a time resolution between 160 ps and 220 ps has been measured depending on the impact position.

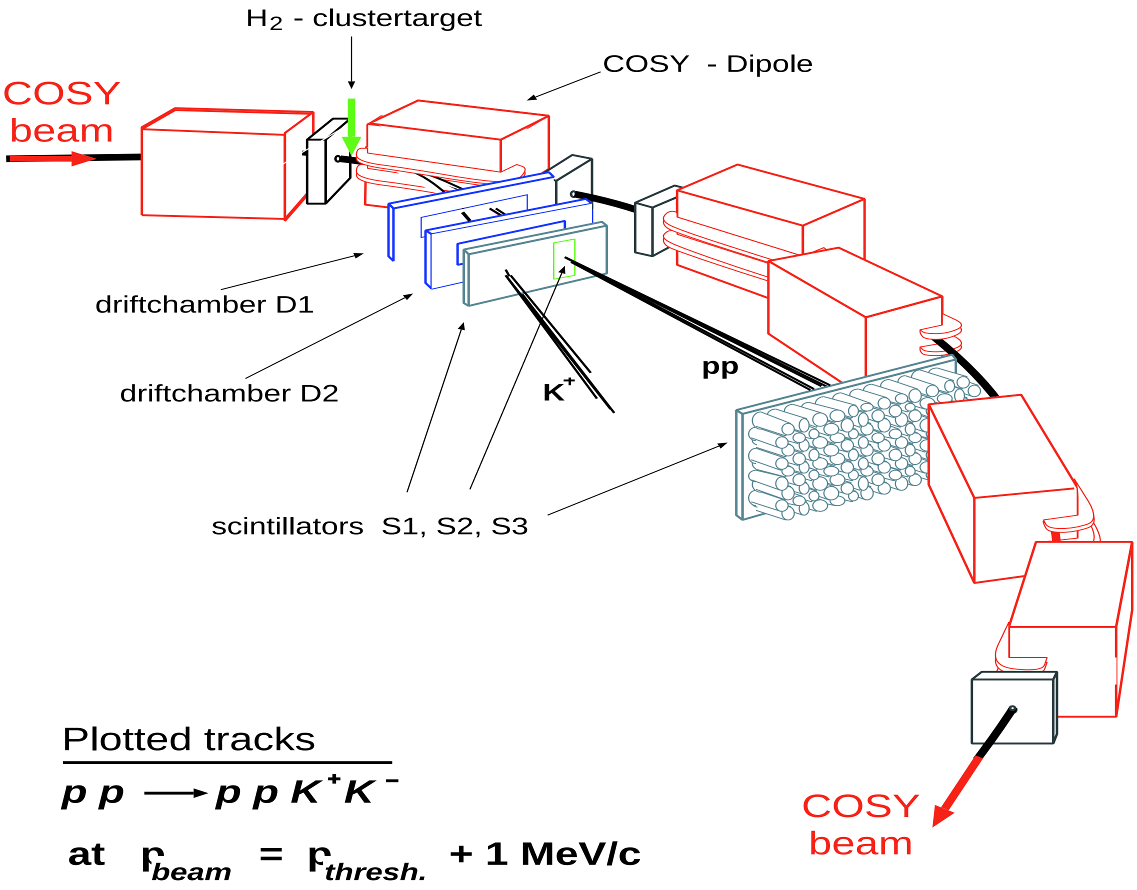

Figure 1.1: Sketch of COSY-11, an internal experimental facility for threshold measurements pp →ppX, where X= π^o,$(\pi^+\pi^-)$,...η',... f_o,...Φ

At a distance of $\sim 9m$ from S1 there is a scintillator wall S3 acting as stop detector for a time-of-flight measurement. It consists of a single scintillator plate $(100 \times 220 cm^2)$ observed by 217 photomultipliers.

The reconstruction of the velocity of particles is made on the base of

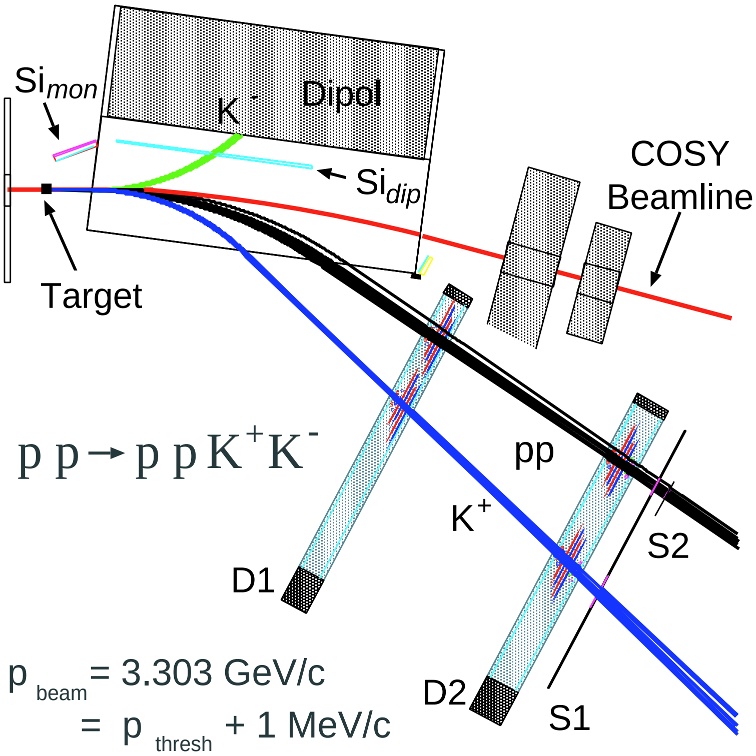

Figure 1.2: Schematic top view of the COSY-11 system

the time-of-flight between the detectors S1 and S3 and the assumption of the particle mass. The result is compared with the measurments of the momentum done by means of the magnetic field.

1.2 Motivation

In general, the aim of this work is to analyse the probability of distinguishing between two cases when one or two particles are passing through a scintillator. The main information about the mechanism of losing energy by the particles and also about the distribution of their energy loss are contained in the first chapter. In the second one the accordance of the experimental data to the Bethe-Bloch formula in the range up to 2 GeV is examined and in the third part the problem of the identification of very close tracks is considered.

'Close' means that the distance of two trajectories is so small that the drift chambers cannot resolve them.

For measurments of the pp$\rightarrow$ppX reactions very close to threshold the momenta of the protons are comparable and their trajectories are very close. With the drift chambers a resolution of two tracks as close as 3 mm is achieved.

For closer tracks a separation via the drift chamber reconstruction is not possible, these are identified as a single track. But such events could be analysed if the particle multiplicity in the scintillator is known, the single track could be interpreted as two tracks with identical momenta and the missing mass of the system X could be calculated.

A multiplicity signal is in principle given by the energy loss in the scintillator.

Due to the energy loss distribution a clear separation of the multiplicity 'one' and 'two' is not efficient with a single scintillation dE/dx signal. The analysis of several scintillator elements is needed.

Chapter 2

Passage of particles through matter

The passage of charged particle through matter [3] is characterized by two principial features:

- loss of energy by the particle,
- a deflection of the particle from its incident direction.

These effects are primarily the result of two processes:

- inelastic collisions with the atomic electrons of the material
- elastic scattering from nuclei

These reactions occur many times per unit path length in matter and it is their cumulative result which accounts for the two principial effects observed. We can separate charged particles into two classes:

- electrons and positrons
- heavy particles: i.e. particles heavier than an electron.

This latter group includes the muons, pions, protons, α-particles and other light nuclei; the heavy nuclei are presently of less interest since at COSY-11 only mesons and baryons with masses less than ^{3}He will be detected. Of the two electromagnetic processes, the inelastic collisions are almost solely responsible for the energy loss of heavy particles in matter. In these collisions ($\sigma = 10^{-17} - 10^{-18}\ cm^2$) energy is transferred from the particle to the atom causing an ionization or excitation of the latter. The amount of energy transferred in each collision is generally a very small fraction of the particle's total kinetic energy: however, in normally dense matter, the number of collisions per unit path length is so large, that a substantial cumulative energy loss is observed even in relatively thin layers of materials. Elastic scattering process occur frequently also although not so often as electron collisions. In general, very little energy is transferred in these collisions since the masses of the nuclei of most materials are usually large compared to the mass of the incident particles. Nevertheless, the major part of the energy loss is still due to atomic electron collisions.

The inelastic collisions are, of course, statistical in nature, occuring with a certain quantum machanical probability. However, because their number per macroscopic path length is generally large, the fluctuations in the total energy loss are small and one can meaningfully work with an average energy loss per unit path length. This quantity, often called the stopping power or simply dE/dx, was first calculated by Bohr using classical arguments and later by Bethe, Bloch and others using quantum mechanics.

2.1 Bethe - Bloch Formula

The energy loss can be calculated using the equation:

$$-dE/dx = 2\pi N_a r_e^2 m_e c^2 \varrho \frac{Z}{A}\frac{z^2}{\beta^2}[ln\frac{2m_e\gamma^2c^2\beta^2T_{max}}{I^2} - 2\beta^2], \qquad (2.1)$$

which is commonly known as Bethe-Bloch formula and is the basic expression used for energy loss calculations. T_{max} is the maximum kinetic energy which can be imparted to a free electron in a single collision, and I is the mean excitation energy, Z and A are the atomic number and the atomic mass of the medium, and ϱ is the matter density. The units are chosen so that dx is measured in mass unit per area, e.g. gcm^{-2}. The other symbols are resumed below:

$m_ec^2 = 0.51099906(15)\ MeV-$ electron mass $\times\ c^2$,
$r_e = 2.81794092(38)\ fm$ – classical electron radius,
$N_A = 6.0221367(36){\times}10^{23}\ mol^{-1}$ – Avogadro's number.

In practice, however, two corrections are normally added: the density effect correction δ, and the shell correction C, so that

$$-dE/dx = 2\pi N_a r_e^2 m_e c^2 \varrho \frac{Z}{A}\frac{z^2}{\beta^2}[ln\frac{2m_e\gamma^2c^2\beta^2T_{max}}{I^2} - 2\beta^2 - \delta - 2\frac{C}{Z}] \quad (2.2)$$

The maximum energy transfer is produced by head-on or knock-on collisions. For an incident particle of mass M, kinematics gives

$$T_{max} = \frac{2m_e c^2\beta^2\gamma^2}{1 + 2\gamma\frac{m_e}{M} + (\frac{m_e}{M})^2} \quad (2.3)$$

if M >> m_e

$$T_{max} = 2m_e c^2\beta^2\gamma^2 \quad (2.4)$$

A minor dependence on M at the highest energies is introduced through T_{max}, but for all practical purposes in high-energy physics dE/dx in a given material is a function of β only. Except in liquid hydrogen, particles of the same velocity have very similar rates of energy loss in different materials.

For particle moving more slowly than atomic electrons, the dE/dx is dominated by the overall $1/\beta^2$ factor and decreases with increasing velocity until about $\beta = 0.96$, where a minimum is reached. Particles at this point are known as minimum ionizing particles (MIP's). As the energy increases beyond this point, the term $\ln(\beta^2)$ becomes almost constant and dE/dx rises again due to the logarithmic dependence (1.1). For $0.4 > \beta > 0.9$ $dE/dx \sim \beta^{-\frac{5}{3}}$ provides a very good approximation.

The bulk of the energy loss results in the formation of positive ions and electrons in the medium. One can distiguish two stages to this process. In the first stage, the incident particle produces primary ionization in atomic collisions. The electrons knocked out in this process have a distribution in energy E' roughly of the form $\Delta E'/(E')^2$: those of higher energy (called δ-rays) can themselve produce fresh ions in traversing in medium (secondary ionization). The resultant total number of electron–ion pairs is 3-4 times the number of primary ionizations. And is proportional to the energy loss of incident particle in the medium. The quantity $(dE/dx)\delta x$ is the mean energy loss via interaction with electrons in a layer of the medium with thickness δx. For finite δx there are fluctuations in the actual energy loss. The large fluctuations in the energy loss are due to the small number of collisions involving large energy transfers. This so-called Landau distribution around the mean value is therefore assymetric with a tail extending to values much larger than the average.

2.2 Energy loss distribution

The energy loss distribution depends on the thickness of the layer.

2.2.1 Thick absorbers

For relatively thick absorbers, where the number of collisions is large the energy loss distribution is Gaussian in form.

$$f(x,\Delta) \sim exp(\frac{-(\Delta-\bar{\Delta})^2}{2\sigma^2}) \tag{2.5}$$

with: x - thickness of absorber, Δ - energy loss in absorber, $\bar{\Delta}$ - mean energy loss, σ - standard deviation.

For nonrelativistic particle the standard deviation is given by:

$$\sigma_o^2 = 4\pi N_a r_e^2 (m_e c^2)^2 \rho \frac{Z}{A} x = 0.15699 \frac{Z}{A} x \tag{2.6}$$

and for relativistic particle the standard deviation can be described as a function of the velocity i.e. i.e.

$$\sigma^2 = \frac{1-\frac{1}{2}\beta^2}{1-\beta^2}\sigma_o^2 \tag{2.7}$$

2.2.2 Thin absorbers

Basic theoretical calculation were made by Landau [5] and Vavilov [6]. The distinguishing parameter in those theories is the ratio

$$\kappa = \frac{\xi}{T_{max}} \tag{2.8}$$

where

$$\bar{\Delta} = \xi = 2\pi N_a r_e^2 m_e c^2 \rho \frac{Z}{A}\frac{z^2}{\beta^2} x \tag{2.9}$$

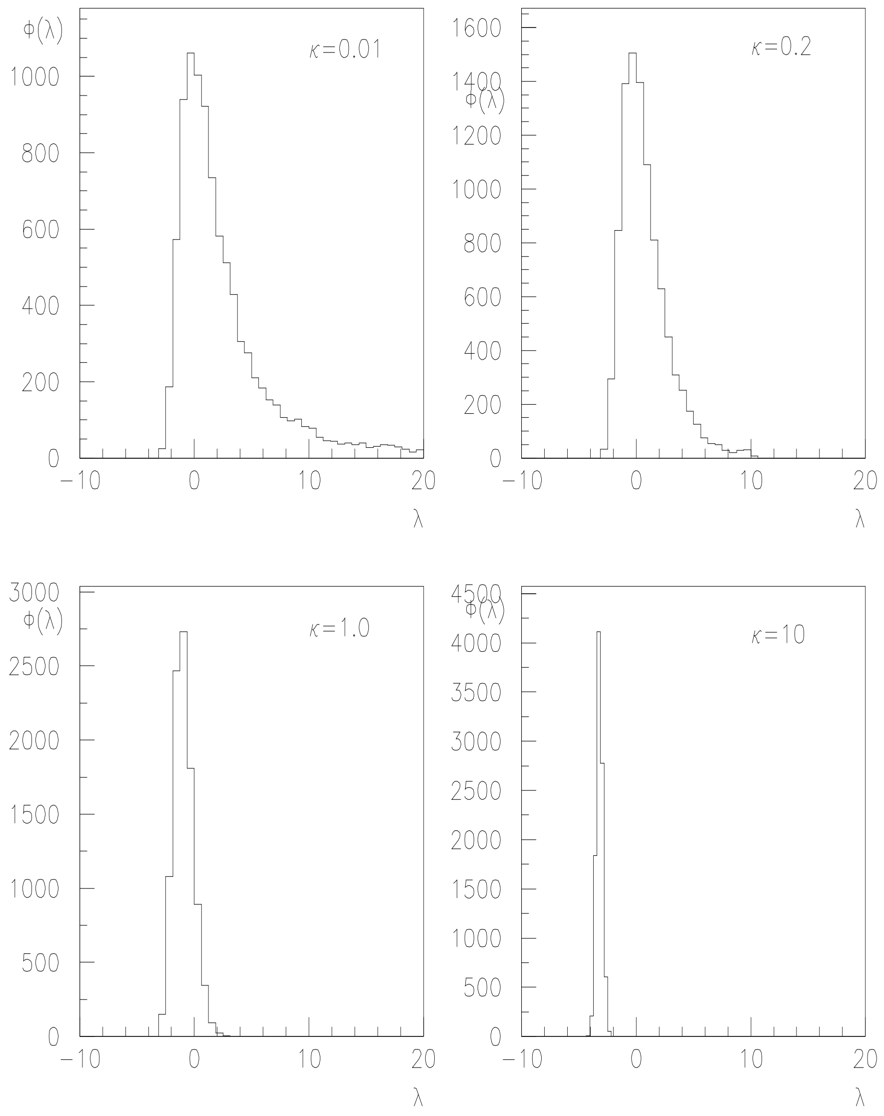

Figure 2.1: Vavilov distributions for various κ as a function of λ. All graphs are prepared for the same value of β=0.5.

The equation (2.5) describes the ratio between the mean energy loss and the maximum energy transfer allowable in a single collision. For $\kappa > 1$ the distribution begins to be Gaussian in shape (for thick absorbers) and for $\kappa < 0.01$ we obtain Landau distribution. The Fig.2.2 shows Vavilov distribution for the different values of κ.

2.3 Landau distribution

For thin absorbers the distribution of energy loss is well described by the Landau distribution. Note that the mean energy loss no longer corresponds to the central peak but is displaced because of the high energy tail. In contrast, the position of the peak now defines the most probable energy loss.

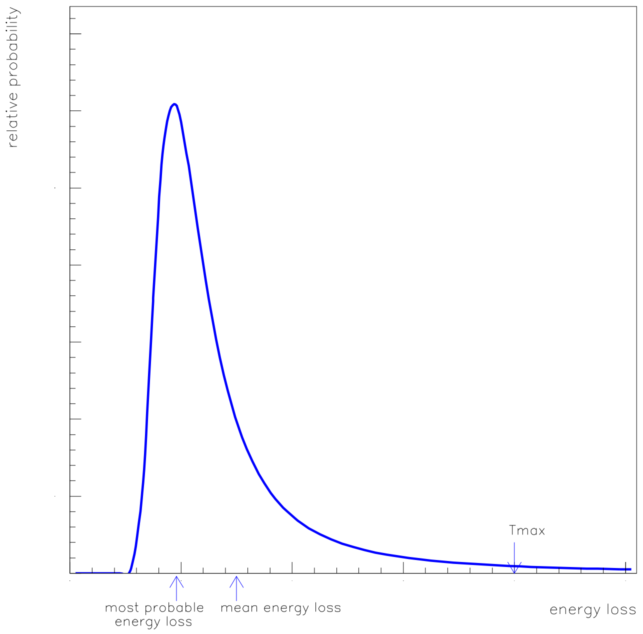

Figure 2.2: Typical distribution of energy loss for a thin absorber.

Landau in his theory made the following assumptions:

- the maximum energy transfer is permitted to be infinite, $T_{max} \to \infty$, in essence taking $\kappa \to 0$,
- the individual energy transfers are sufficiently large such that the electrons may be treated as free. Small energy values from so-called distant collisions are ignored,
- the decrease in velocity of the particle is negligible i.e. the particle maintains constant velocity.

This distribution is expressed as

$$f(x, \Delta) = \frac{\Phi(\lambda)}{\xi} \tag{2.10}$$

where

$$\Phi(\lambda) = \frac{1}{\pi} \int_0^1 exp(-u \ln u - u\lambda) \sin \pi u du \tag{2.11}$$

$$\lambda = \frac{1}{\xi}[\Delta - \xi(\ln \xi - \ln \varepsilon + 1 - \gamma)] \tag{2.12}$$

$\gamma = 0.577.../Euler'sConst/$

$$\ln \varepsilon = \ln \frac{(1-\beta^2)I^2}{2mc^2\beta^2} + \beta^2 \tag{2.13}$$

The function $\Phi(\lambda)$ is an universal function dependent only on the parameter λ and must be evaluated numericaly. From the evaluation of $\Phi(\lambda)$, the most probable energy loss is found to be

$$\Delta_{mp} = \xi[\ln \frac{\xi}{\varepsilon} + 0.198] \tag{2.14}$$

Chapter 3

Stopping power in scintillation detectors

For particles such as protons, it is often stated that $|dE/dx|$ falls as β^{-2} before reaching the broad minimum at $\beta\gamma \approx$ 3.0-3.5. In fact the slope is nowhere this great and $|dE/dx|\sim \beta^{-\frac{5}{3}}$ provides a very good approximation to the actual function.

In this chapter we want to show that this situation really takes place and the energy loss in the range of relativistic velocities lower than β=0.9 could be described by a simple analytic function being in the accordance with the Bethe-Bloch formula.

For this purpose two kinds of data were examined: semi-experimental data contained in the ICRU Report and experimental data from the COSY-11 experiment (pp$\rightarrow$ppη', Sep. 1996).

3.1 ICRU Data

At first we want to present the results considering the data contained in the ICRU Report [2] (International Comission On Radiation Units And Measurement Report). There one can find values of stopping power for protons, pions, etc. in different materials. These numbers are based on Bethe's stopping power theory with semi-empirical mean excitation energies and shell corrections, and with corrections for departures from the first Born approximation.

The presented example considers the results for protons in plastic scintillator (vinylotoluen-based). This kind of scintillation material is especially interesting because it is closest to the one used for building the detectors S1 and S2. The range of the energy between 0.045–2.0 GeV was chosen.

As we know in this range of energy one can expect the energy loss as a function of velocity in the form

$$f(x) \sim x^{-\frac{5}{3}} \tag{3.1}$$

The dependance dE/dx versus velocity was made and the function (3.2) was fitted. The results are shown in Fig.3.1. The coefficients are resumed in the table 3.1.

$$f(x) = p_1 \cdot x^{p_2} + p_3 \tag{3.2}$$

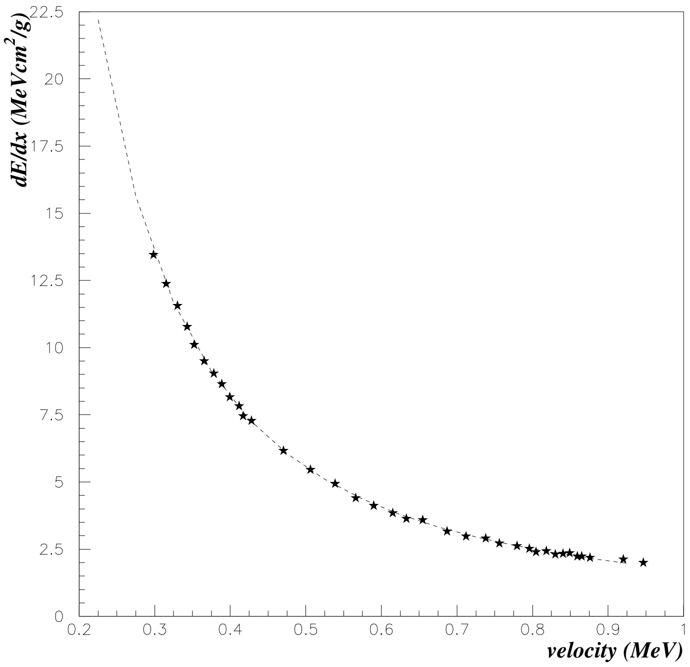

Figure 3.1: Stopping power as a function of β for protons in plastic scintillator.

p_1	p_2	p_3
1.594	-1.761	0.141

Table 3.1: The coefficients of the fitted function (3.2) to the ICRU data.

3.2 Scintillators BC-404

Organic scintillators utilize the ionization produced by charged particles to generate optical photons, usually in the blue to green wavelenght regions. Plastic scintillators are by far the most widely used. Typical photon yields are about 1 photon per 100 eV of energy deposit. A one-cm-thick scintillator traversed by a minimum-ionizing particle will therefore yield $\sim 2\times10^4$ photons. The resulting photoelectron signal depends on the collection and transport efficiency of the optical package and the quantum efficiency of the photodetector. Decay times are in the ns range and risetimes are much faster.

3.2.1 Scintillation mechanism

A charged particle hits the scintillating material, and traversing matter causes ionization and excitation of molecules. Certain types of molecules, however, will release a small fraction ($\sim 3\%$) of this energy as optical photons. This process called scintillation is especially marked in those organic substances which contain aromatic rings such as polystyrene, polyvinylotoluene, and naphtalene. A part of the emitted photons travels to the edge of the scintillator and from here by means of a light guide is transported to the photomultiplier. The first step in the photomultiplier is converting light into a weak photoelectron current and next to amplify it. The outgoing signal is then analyzed by the electronics system.

The plastic scintillators used in high-energy physics are binary or ternary solutions of selected fluors in a plastic base [7]. Fluors are used as "waveshifters" to shift scintillation light to a more convenient wavelength. The absorption and emission are spread out over a wide band of photon energies and have some overlap, that means some fraction of the emitted light can be re-absorbed. This self-absorption is undesireble for detector applications because it causes a shortened attenuation length.

Both scintillation detectors S1 and S2 are BC-404 plastic scintillators

	S1	S2
	plastic scintillator BC-404	
material	polyvinylotoluen	
thickness [mm]	4	2
density [g/cm^3]	1.032	1.032

Table 3.2: The chosen properties of the scintillator BC-404.

(the basic properties are resumed in the table 3.2). BC-404 is a ternary plastic scintillator. That means that in the base material two admixtures are dissolved. In this case the base material is polyvinylotoluen. It scintillates also as pure material, but its light output is relatively low. This ability is improved by dissolving therein a small amount (few percent) of an aromatic compound called primary solute. Such solution has to be used in small quantities, to prevent reabsorption. The second additive (secondary solute) allows to get rid of this disadvantage by shifting the emitted light to a longer wavelength.

3.2.2 Stopping power in the detectors S1 and S2

In this section the COSY-11 experimental data are presented. In the Fig.3.2 the example of the distribution of energy loss for protons versus relativistic velocity β is shown for all segments in S1.

A similar spectrum was obtained for the detector S2. The reconstruction of velocity is made on the base of the time-of-flight between the detectors S1 and S3. In the Fig.3.3 the spectrum of the velocity of the examined particles is shown. One can observe a certain number of entries above 1, these are out of the physical range and are is caused by the reconstruction method used. The velocity is reconstructed on the base of the time-of-flight, which has a certain distribution, caused e.g. by transit spread in the photomultipliers. In further consideration the range of β between 0.4–1.0 is chosen. Both scintillation hodoscopes can be treated as rather thin layers (thickness of S1 is 4 mm and of S2 is 2 mm). This means that for certain values of velocity the energy loss is well described by the Landau distribution.

The data measured at a beam momentum of p_b=3.214 GeV were analysed

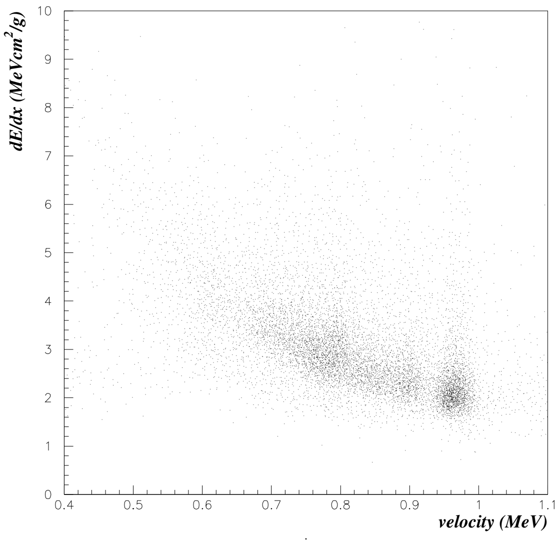

Figure 3.2: Energy loss spectrum for all segments of S1.

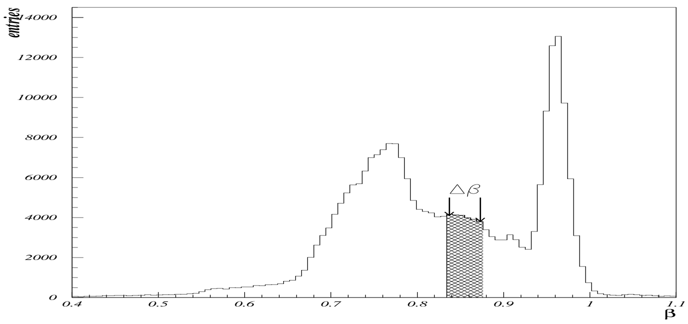

Figure 3.3: The reconstructed velocity of the examined particles.

for both scintillators S1 and S2. The events were selected inside velocity of $\Delta\beta$=0.035 width, and for each bin the energy loss spectra were accumulated, and the Landau curves were fitted for each spectrum.

An example of such a distribution is shown for β=0.75 in Fig.3.4. One can see that according to the theory the distribution is skewed towards high values. The dependence of the energy loss on the velocity in the form (Eq.

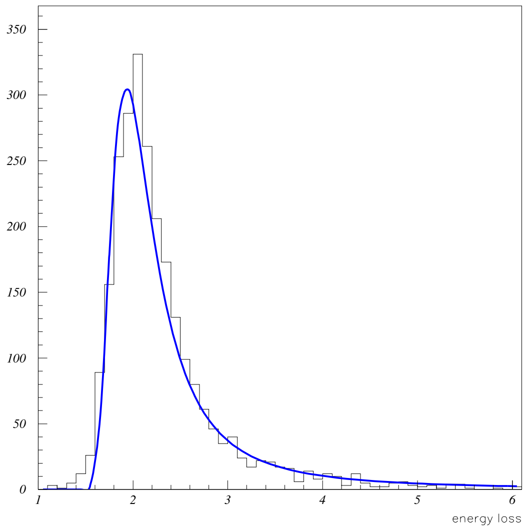

Figure 3.4: For a given value of velocity β (in this case β=0.75) a Landau distribution for the energy lost by the particles is observed.

3.2) is expected.

On the base of the chosen spectra, by means of values of the most probably energy loss (maximum of Landau distribution), the dependance of stopping power on velocity was reconstructed (see Fig.3.5). To those points the function (3.2) was fitted. The values of respective coefficients are in the table 3.3.

	p_1	p_2	p_3
S1	1.648	-1.667	0.178
S2	1.788	-1.709	-0.197

Table 3.3: The coeffitients of the fitted function (3.2) to the experimental data

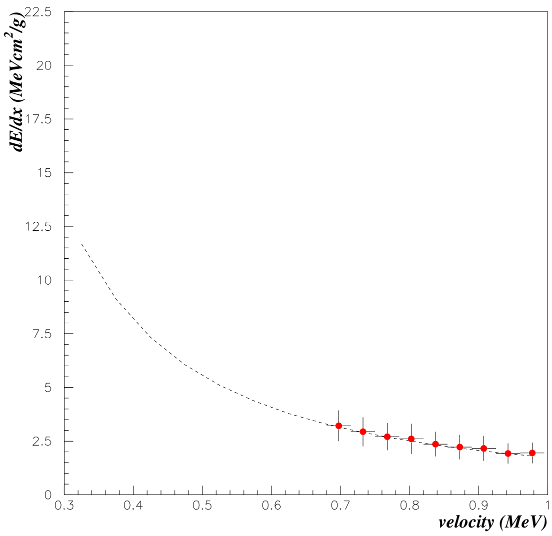

Figure 3.5: The stopping power as a function of relativistic velocity for all segments in S1.

Chapter 4

One and Two Particle Events Identification

One of the basic requirements of experimental particle physics is the determination of particle trajectories.

For a long time all tracking devices were optical in nature. The year 1968 brought huge changes because of Charpak's invention. In the COSY-11 installation trajectories of both protons and positively charged mesons are measured by two planar drift chamber stacks. These are spaced by 80 cm. One of them contains six, the second eight detection planes. The planes are as follow: two with vertical wires, two with wires inclined by $+31^o$ and two inclined by -31^o. The wires in consecutive planes of each pair are staggered by half of the cell width in order to resolve the left-right position ambiguity with respect to the sense wire. In the second chamber stack there are two additional planes with vertical wires in order to improve the position resolution in the horizontal direction. The chosen configuration of the detection planes allows to measure the horizontal and vertical coordinates and enables a unique identification of multihit events.

For typical wire chambers the efficiency for charged particle detection is very high with values in the order of $98 - 99\%$. The position resolution of drift chambers is 250 μm and 500 μm respectively, the usual drift region is about 4 cm. But if the trajectories of two particles are closer than 3 mm the drift chambers cannot resolve them.

The problem of the identification of one and two particle events is of interest in this chapter.

4.1 Analog signals

An analog signal carries continuously-valued information by varying one or more of its characteristics (e.g. amplitude and/or shape), in some fixed relation to the information value. A scintillation detector generates pulses whose amplitudes are in proportion to the energy deposited in the detector. If a beam of particles with a continuous spectrum of energies is allowed to strike the detector, then a continuous analog spectrum of pulse heights will result. More generally, if we consider each possible amplitude or shape of pulse as a state, then the analog signal can be said to have an infinite number of states. In nuclear physics, most analog pulses are of the amplitude varying type, although in certain cases, information is also contained in the shape of the pulse. Since the proportionality between pulse height and energy is usually linear, these pulses are also referred to as linear pulses.

4.2 Analog Digital Converter

The ADC is a device which converts the information contained in an analog signal to an equivalent digital form. This instrument is the fundamental link between analog and digital electronics. To give an example of its range, suppose an ADC accepts input pulses in the range of 0 to 10 V and is capable of outputting digital numbers from 0 to a maximum of 1000.

An input signal with an amplitude of 2.5 V would convert to the digital number 250. Similarly, for a 150 mV pulse, we would find 15, and so on. The resolution of the ADC depends on the range of digitalization. If numbers between 0 and 10,000 were generated instead of 0 and 1000 a finer digitalization and the higher resolution would be obtained.

ADC's may be of two types: peak-sensing or charge sensitive. In the first the maximum of the voltage signal is digitized, as in the above example, in the second one it is total integrated current.

The charge sensitive type is used with current-generating devices, e.g. a photomultiplier in current mode (usually fast detectors). Peak-sensing is used with slower signals which have already been integrated. The time of integration or the time period over which the ADC seeks a maximum is usually determined by the width of a gate signal.

Electronically many methods are in current use for analog to digital conversion. In the case of the ADC used in the COSY-11 setup the ramp or

Wilkinson method is used.

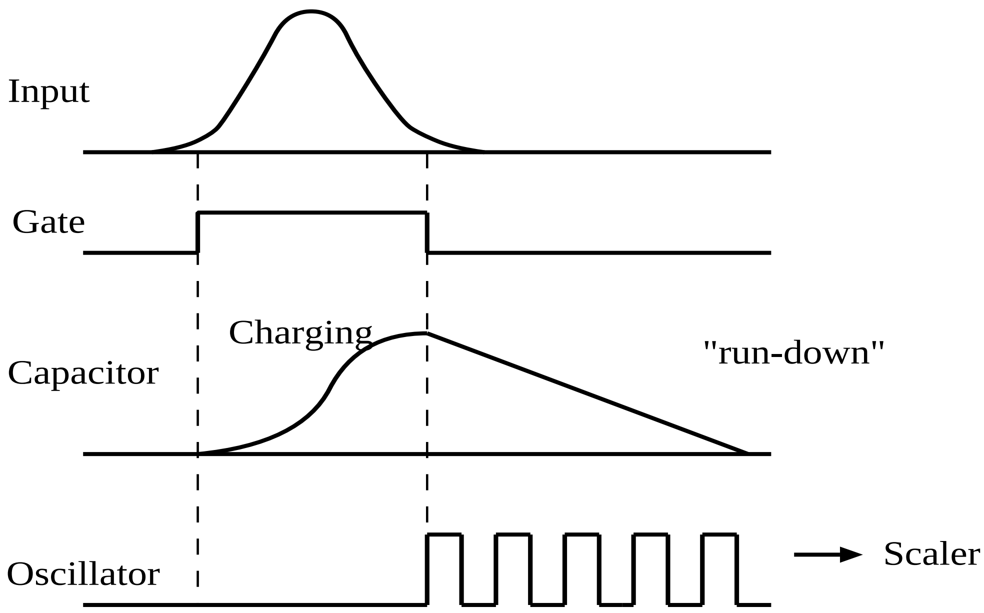

Figure 4.1: Illustration of rising of ADC signal.

In this technique, the input signal is first used to charge a capacitor. This capacitor is then "run down" i.e. discharged at a constant current. At the start of the discharge, a scaler counting the pulses from a constant frequency clock or oscillator is started. When the capacitor has completly discharged, the scaler is stoped. The content of the scaler is then a number proportional to the charge on the capacitor.

The time required for the digitization process is called the conversion time.

In the Wilkinson method the conversion time needed is covenned by the frequency of the clock. Obviously, the faster the clock, the faster the ramp can be run down.

4.3 Calibration

The output signal of a scintillation detector is a current pulse. The amount of ionization is then proportional to the electrical charge contained in this signal.

The light output from the scintillator segments in the COSY-11 setup is read out by two phototubes, from up and down side. The photon output signals are then digitized by ADCs, delivering the values ADC$_{up}$ and ADC$_{down}$. The signal is proportional to the energy lost by the particle.

The energy loss can be expressed by the formula:

$$\Delta E = (ADC_{up} + ADC_{down})/2 \tag{4.1}$$

A calibration was done for particles passing the central part of the scintillator module with velocity β = 0.65-0.85. This procedure was applied for all channels separately, giving ADC information in MeV units.

4.4 One- and Two- Track Events

By means of knowledge of the magnetic field and position of the particle hit in the drift planes one can reconstruct the trajectories of the reaction products. In the case when trajectories of two particle are closer than 3 mm the drift chambers treat their trajectories as a common trace.

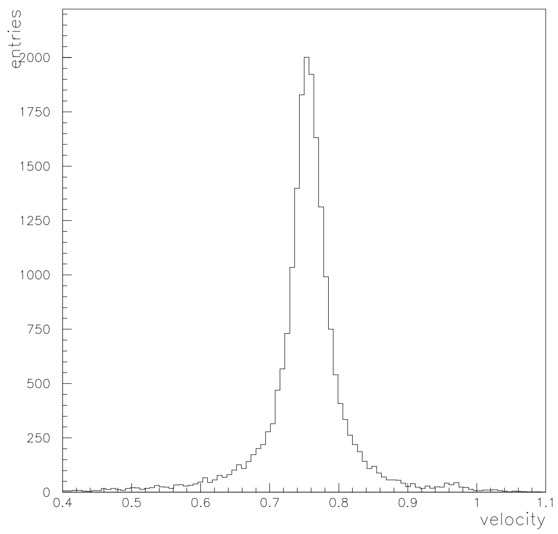

Figure 4.2: The distribution of the velocity of the studied particles.

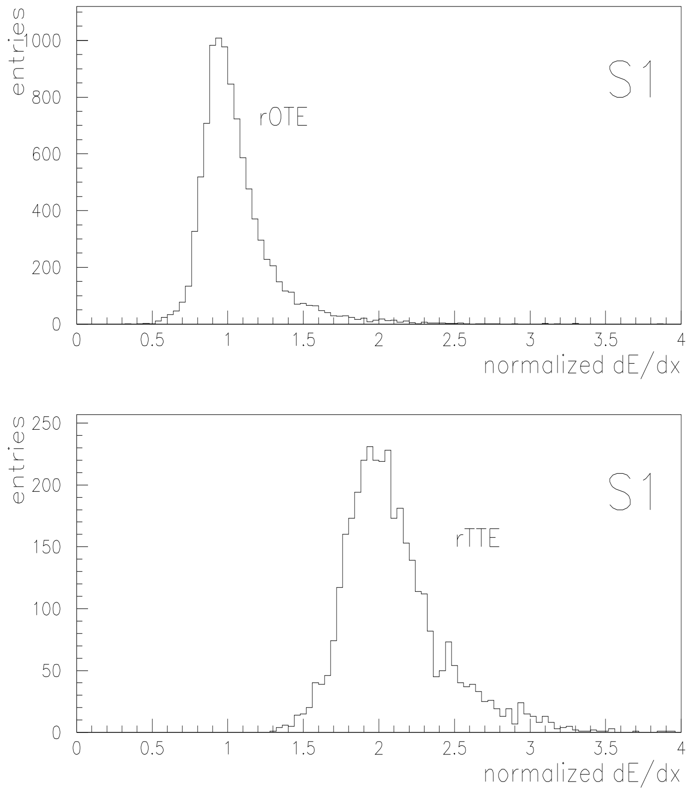

Figure 4.3: The distributions of rOTE (upper picture) and rTTE (lower picture) for S1.

If the particles have a similar velocity, each of them looses nearly the same amount of the energy in the scintillation detector. So one can expect a two times higher energy loss when two particles passed through the scintillation detector. On the base of this information, the separation between two cases should be possible: if one or two particles passed through the scintillation detector.

This method should be examined in comparision to the information about the number of particles resolved in the drift chambers.

In this section two situation are considered:

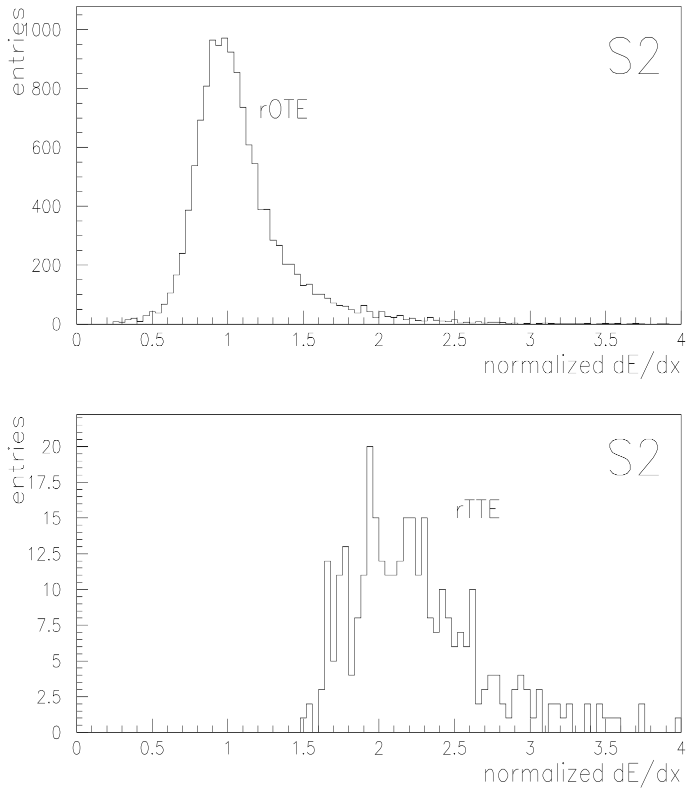

Figure 4.4: The distributions of rOTE (upper picture) and rTTE (lower picture) for S2.

- the drift chambers resolved two particles and the distribution of their energy loss in the scintillation detector is examined,
- the drift chambers registered only one particle, but there is a certain probability that there are two particles with trajectories closer than 3 mm in the drift chambers.

So, the following definitions are introduced:

- the first case: the drift chambers resolved two trajectories and the terms **resolved one track events** (rOTE) and **resolved two track events**

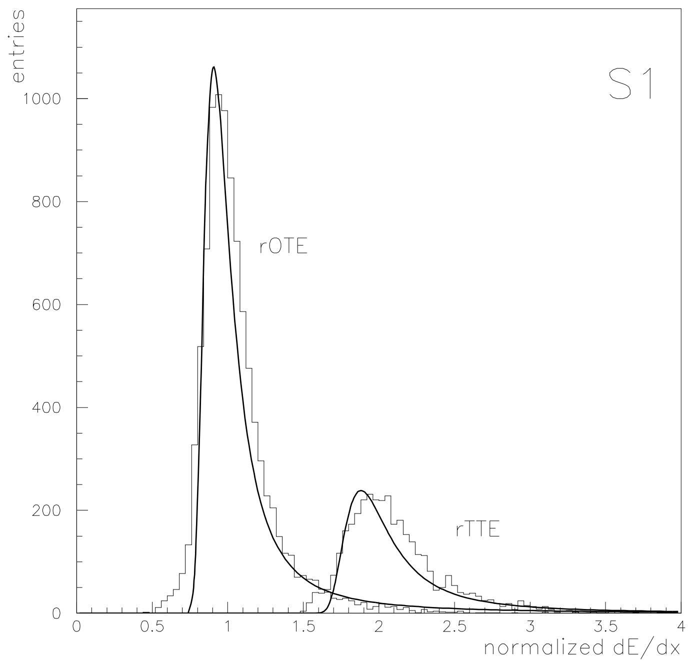

Figure 4.5: The distributions of rOTE and rTTE for S1 together with the fitted Landau functions.

(rTTE) mean that only one or two particles, respectively, passed through a segment in the scintillation detectors S1 or S2,

- the second case: the drift chambers registered only one particle and the terms **non-resolved one track events** (nOTE) and **non-resolved two track events** (nTTE) consider the situation when one expects (on the base of the information about the energy loss) that only one or two particles, respectively, passed through a segment of S1 or S2.

In this section the data (pp$\rightarrow$pp$\eta^{'}$, Sep. 96) at the beam momentum $p_b = 3.214 GeV/c^2$ are presented.

The data were analyzed for OTE and TTE events for selected segments in S1 and all segments in S2. The range of velocity between $\beta = 0.65 - 0.85$ has been chosen (see Fig.4.2). All spectra are normalized so that the 3 MeV energy loss corresponds to the value 1. The scale is linear.

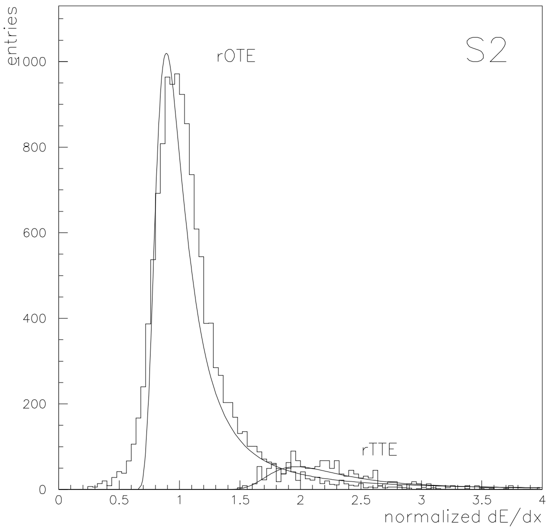

Figure 4.6: The distribution of rOTE and rTTE for S2 with associated Landau functions.

Figure 4.3 shows the situation when the drift chambers resolved two particles. The upper part of the graph shows the distribution of the energy loss for the case where each particle passed through a segment of the scintillation detector. The lower part shows the distribution when two particles passed trough one segment. In Fig.4.5 and Fig.4.6 the spectra of rOTE and rTTE are shown together with fitted Landau functions for S1 and S2, respectively. Figure 4.7 illustrates the distribution of the energy loss in S1 when the drift chambers registered only one particle. One can observe two peaks distributed around the values 1 and 2, and are supposed to be nOTE and nTTE. The same case but for S2 is presented on Fig.4.8

The distribution of the energy loss in both cases represents Landau shapes.

In the same way the spectra for the scintillation detector S2 were prepared.

The difference of S1 and S2 spectra is due to:

- half thickness of S2 in respect to S1 segments leads to broader energy loss distributions,
- the probability of hitting two segments with a 'close' trrack of distance

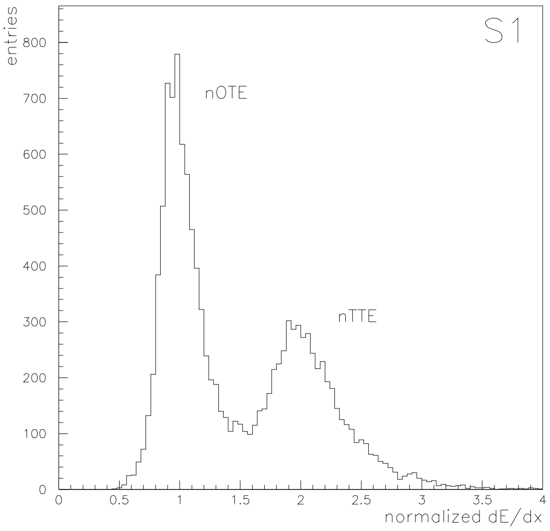

Figure 4.7: The distribution of nOTE and nTTE for S1.

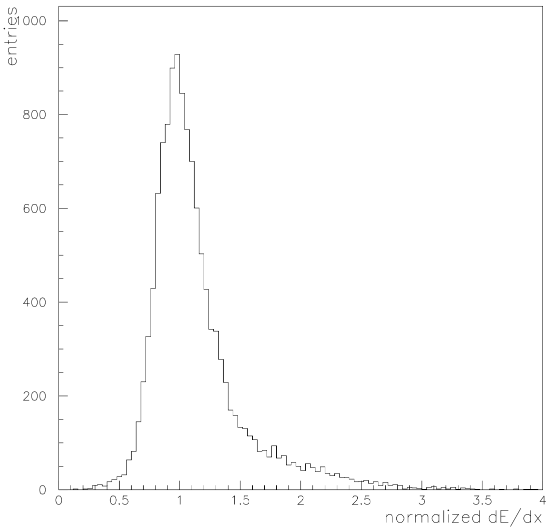

Figure 4.8: The distribution of nOTE and nTTE for S2.

closer than 3 mm in the drift chambers is about 10:1, for S1:S2, that means that the TTE peak in the S2 energy loss spectrum is reduced by a factor 10, which can be obviously seen on Fig.4.5 and 4.6.

Generally, OTE and TTE are distributed around the values 1 and 2 (3 and 6 MeV, respectively), but between these there is a region where both cases are mixed. That means one can recognize an event as OTE or TTE only with certain probability. In order to identify these hypothesis testing should be used.

4.5 Hypothesis testing

Many problems arise in science where a decision must be made to accept or reject a statement about some particular parameter. The statement in this situation is refered to a hypothesis and the decision making process about the hypothesis is termed hypothesis testing.

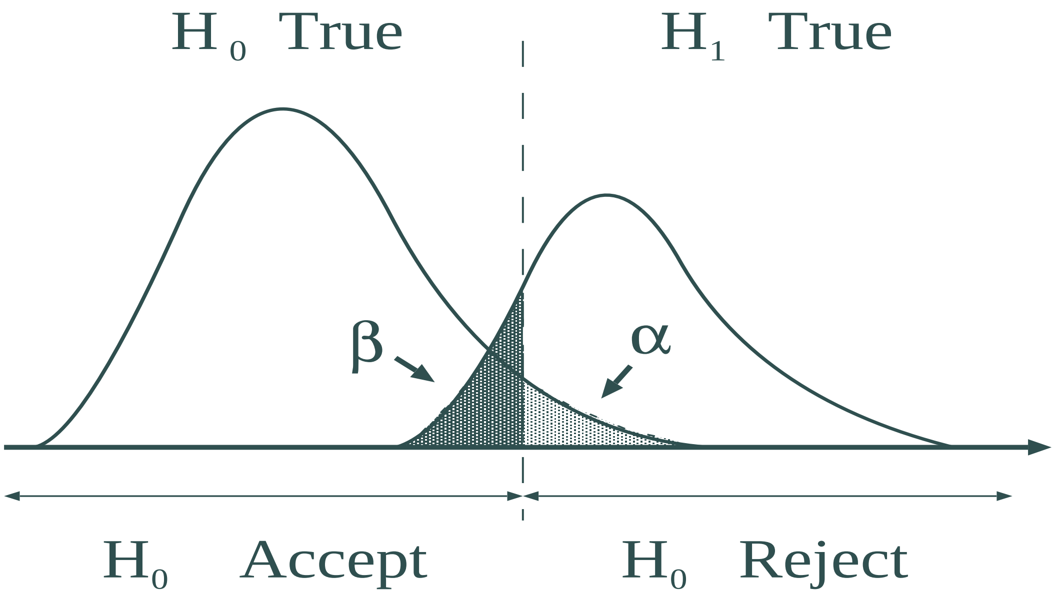

Figure 4.9: Resolution functions of a certain parameter under hypothesis H_o and H_1, with the marked regions of loss (α) and contamination (β), (see page 32).

In every hypothesis testing procedure there are few similar steps: the null hypothesis H_o and the alternative H_1 must be chosen, further the level of 'significence' must be defined. Level of the significance called also size of the test, α can be defined as the probability of rejecting a true null hypothesis. The value of α is typically chosen as 0.1, 0.05, 0.01. Further the test statistic must be collected. In such testing we distinguish two kind of errors:

- error of the first kind (loss) – rejecting the null hypothesis when is true. The probability of such an error is α,

- error of the second kind (contamination)– accepting the null hypothesis when it is false. The probability for making such an error is β.

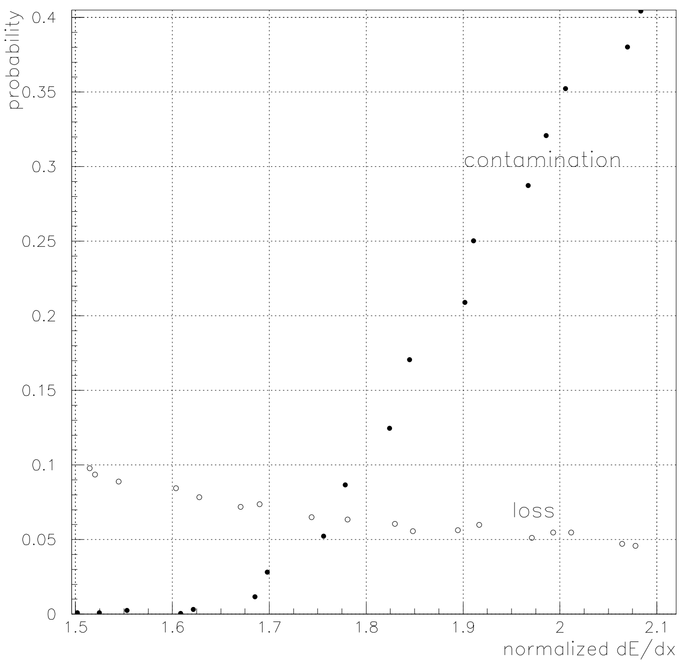

Figure 4.10: Loss and contamination as the function od normalized energy loss in the region where rOTE and rTTE are mixed. Under the null hypothesis H_o the case of rOTE is taken.

In our case the separation of OTE and TTE is based on the energy loss information. The energy loss in scintillator can be chosen as the test statistic.

Under hypothesis H_o one can expect OTE, and under H_1 TTE. Thus the acceptance region would be chosen around value 1 (corresponds to 3 MeV) and the critical region around 2 (6 MeV). True OTE having larger energy, around 6 MeV would be classified as TTE and would constitute the loss. True TTE with energy closer to 3 MeV constitute the contamination to OTE. The exact choice of the critical region depends on how much loss and

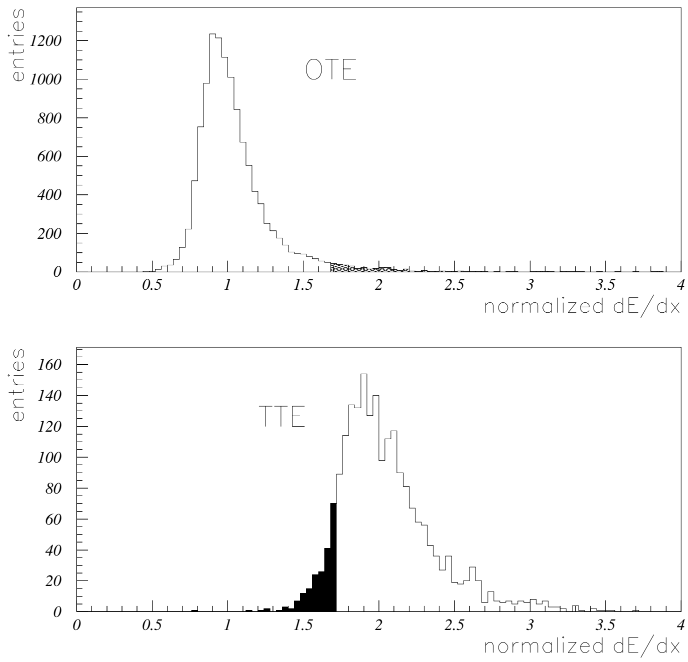

Figure 4.11: The OTE are chosen as the null hypothesis and the significance level is 0.07.

contamination one is willing to accept. Clearly it is desirable to minimize both the loss α and the contamination β.

The Fig.4.10 shows both the contamination and the loss in function of the chosen range of the normalized energy loss, under null hypothesis OTE are chosen. One can see how large is the contamination and the loss in respect to chosen energy cut. It is important also to note that the actual contamination (TTE events accepted as OTE) is expressed as $\beta \cdot$N, where N is the a priori abundance of TTE produced. So a large value of β (while α is small) could be accepted if N is small.

The Fig.4.11 shows both spectra, while OTE is chosen as the null hypothesis and the significance level is 0.07. The loss of OTE 7% but in the same time only 3% of TTE are accepted as the contamination.

Chapter 5

Two-dimensional representation of energy deposits.

In the previous chapter the one-dimensional method of the separation of OTE and TTE was shown. Now, the problem of the distinguishing between those both cases is considered in two dimensions. The presented graphs show the distribution of the energy loss in the scintillation detectors S1 and S2 under the condition that the particles pass both S1 and S2. The graphs are made on the base of the same data mentioned in the previous chapter. The two-dimensional distribution was expected to distinguish in clear way between all OTE and TTE cases.

All spectra are made for all segments of S2 and the corresponding segments of S1.. Figure 5.1 shows the distribution of the energy loss in S1 versus the distribution of the energy loss in S2 (for the case when the drift chambers registered two particles). In this picture the strong peak (nOTE) is easily observed and a very small one in the place expected to be rTTE. The Fig.5.2 shows only rTTE.

The similar graphs are made for the case when the drift chambers registered only one particle.

The Fig.5.3 shows both cases nOTE and nTTE together. On the next figure (see Fig.5.4) the peak of all those cases which are expected to be nTTE is shown.

The both histograms for TTE (5.2 and 5.4) are made by requiring at least an energy deposit of 1.5 in S1 and S2 (equivalent to 4.5 MeV).

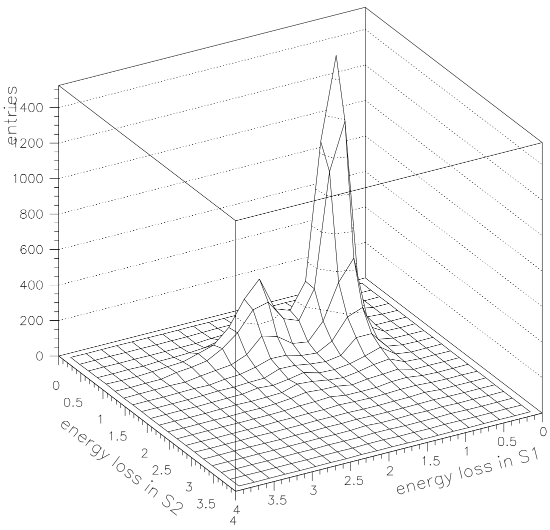

Figure 5.1: Two-dimensional graph for the distribution of the energy loss in the scintillation detectors S1 and S2 (rOTE and rTTE).

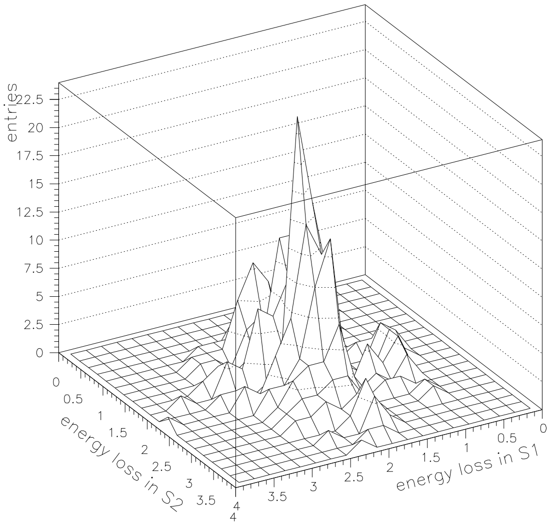

Figure 5.2: Two-dimensional graph for the distribution of the energy loss in the scintillation detectors S1 and S2 (only rTTE for the energy cut in 1.5).

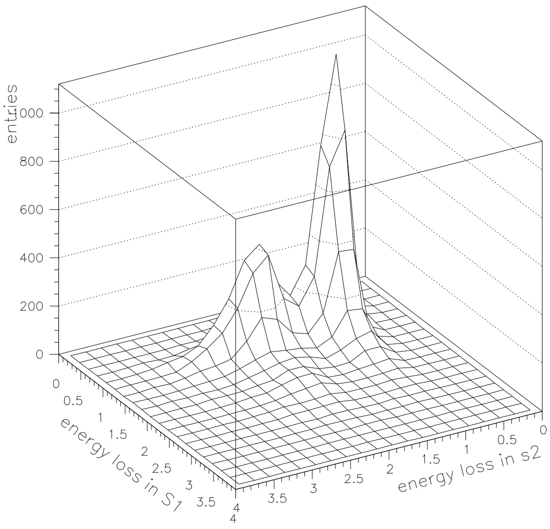

Figure 5.3: The distribution of the enrgy loss in the case that the drift chambers registered only one particle (nOTE and nTTE together).

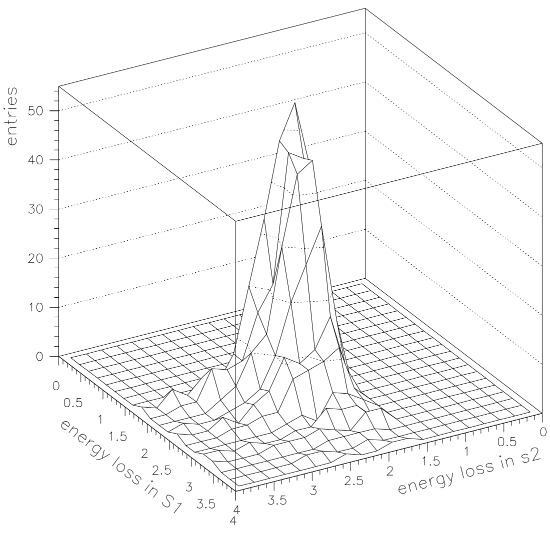

Figure 5.4: All nTTE for the energy cut in 1.5.

Figure 5.5 shows TTE for different energy cuts (1.6, 1.5, 1.4, 1.3). In all cases it can be seen easily that there is no clear minimum between the area expected to be TTE and the surrounding.

The lack of the clear minimum is also obviously shown in Fig. 5.6 and 5.8.

As one can see the usage of the two-dimensional method does not produce a clear separation between OTE and TTE.

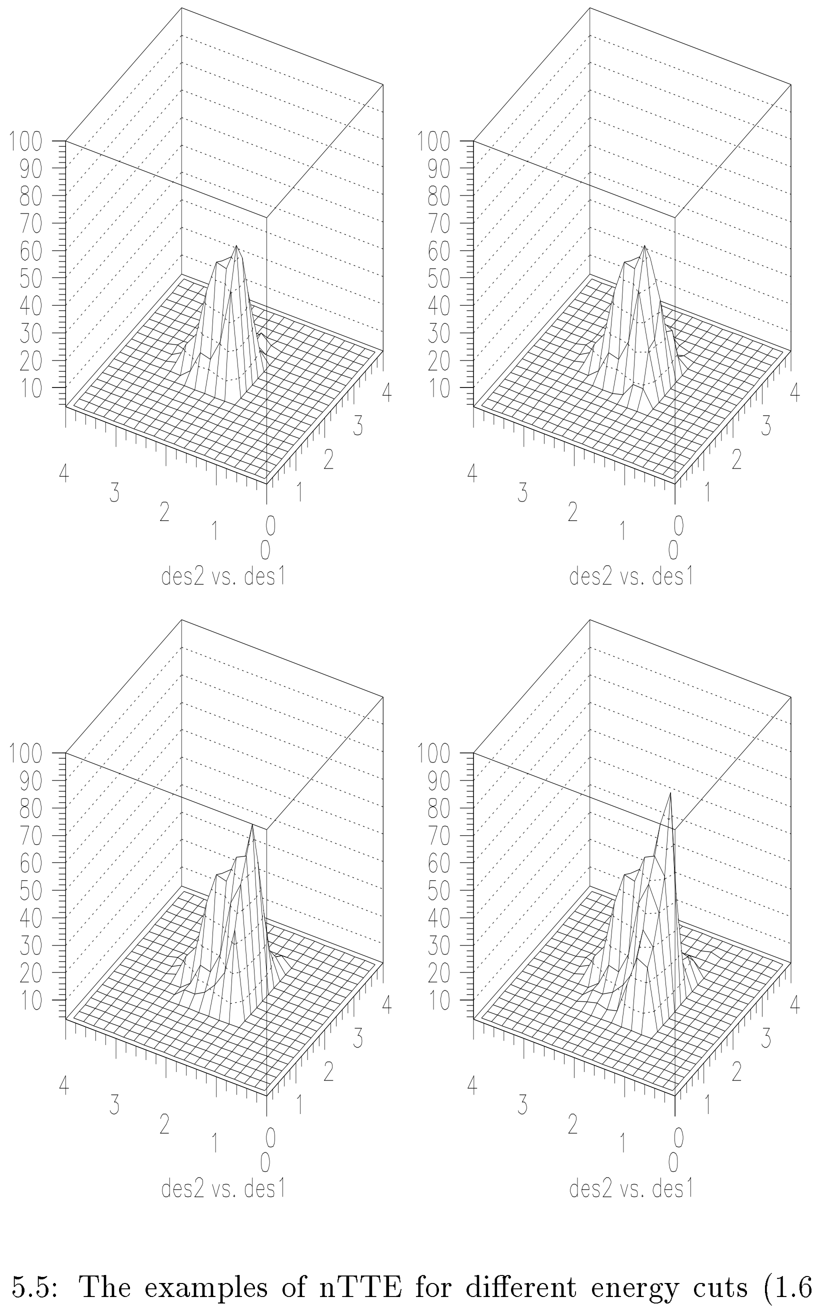

Figure 5.5: The examples of nTTE for different energy cuts (1.6, 1.5, 1.4, 1.3, respectively).

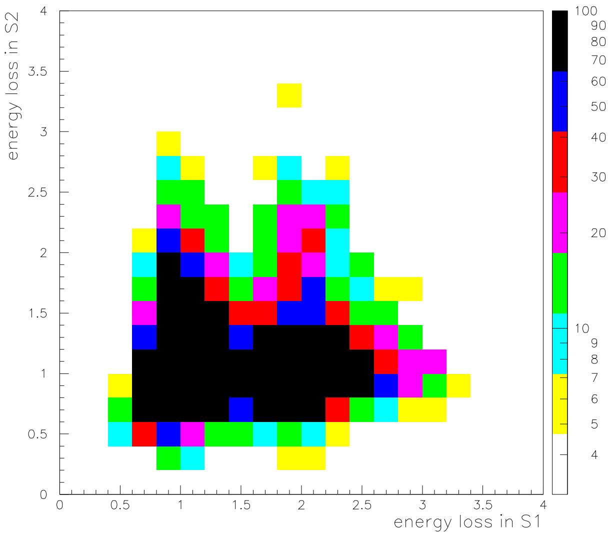

Figure 5.6: Two-dimensional distribution of the energy loss for both S1 and S2 in the case when the drift chambers registered two particles.

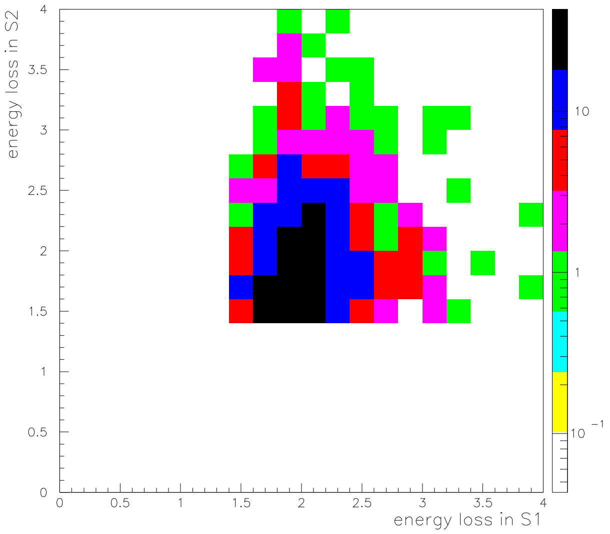

Figure 5.7: The area of the rTTE for energy cut in 1.5.

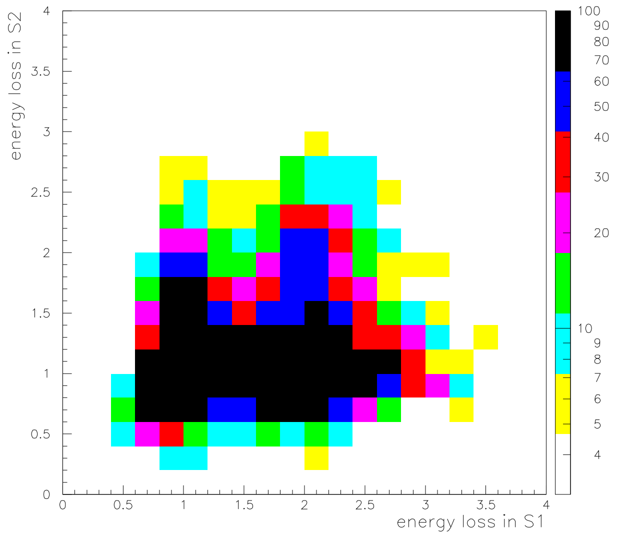

Figure 5.8: Two-dimensional energy loss for both S1 and S2 in the case when only one particle is reconstructed via the drift chambers.

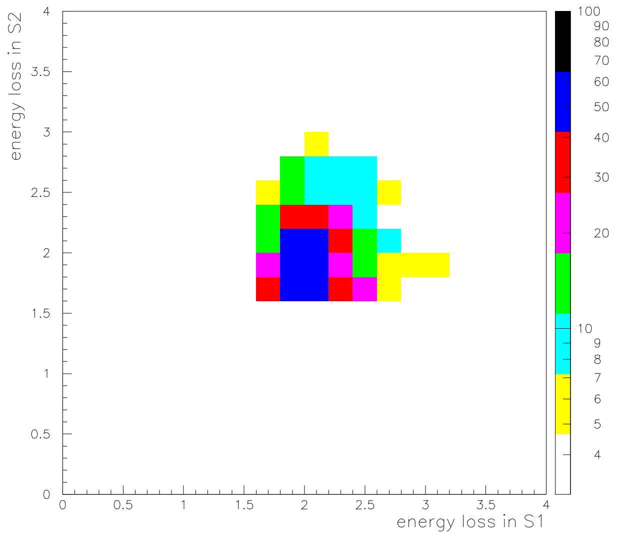

Figure 5.9: The expected area of nTTE for energy cut in 1.5.

Conclusions

This work shows that the energy loss distribution in the scintillation detectors S1 and S2 is well described by the Landau distribution.

The possibility of describing the Bethe-Bloch formula by the simple analytic function in the range up to β=0.9 was examined by means of the energy loss distribution for several values of β (Landau distributions).

The coefficients of this function were calculated and the accordance to the theoretical Bethe-Bloch formula was obtained.

Further, the problem of the separation between one and two particles passing through a scintillator was studied.

In the one-dimensional representation the separation between both cases performes well, one can see that with an energy cut at 4.5 MeV the one and two track events can be separated. The accepted area of two track events is contaminated with 7% of single tracks, while 3% of two track events are loss. For the S2 scintillator the obtained results are not so clear due to its worse energy loss resolution.

The two-dimensional representation of the energy loss distribution was expected to separate between single and double tracks clearly, but because of the worse energy resolution in S2 does not bring the expected results.

Acknowledgemets

I would like to thank Prof. L.Jarczyk and Prof. B.Kamys for guiding me through my studies at the Jagiellonian University in Cracow and giving the possibility of doing my diploma work in Jülich.

I appreciate the support given by Prof. K.Kilian for a very interesting time at the Institute of Nuclear Physics in Forschungszentrum in Jülich.

I very much enjoyed my work within the COSY-11 collaboration. Thank to all group members, especially to Walter Oelert.

Bibliography

[1] W.T.Eadie, D.Drijard, F.E.James, M.Ross, B.Sadoulet *Statistical Methods in Experimental Physics*, North Holland, 1971

[2] ICRU Report, *Stopping Powers and Ranges for Protons and Alpha Particles*, Maryland, USA, 1993

[3] W.R.Leo, *Techniques for Nuclear and Particle Physics Experiments*, Springer, Berlin, 1992

[4] Collaboration of the COSY-11 Installation, *COSY-11 an Internal Experimental Facility for Threshold Measurments*, KFA-IKP(1)-1995-1

[5] L.Landau, J.Phys(USSR), 8, 201(1944)

[6] P.V.Vavilov, Sov.Phys, JETP, 5, 749(1957)

[7] P.Moskal, *Response Function of The Trigger Scintillation Detector for The COSY-11 Installation*, KFA IKP, Jülich-2828, 1993

[8] Physical Review D, *Particles and Fields*, Vol. 50, Am. Phys.Soc (1994)

[9] B.Rossi, *High Energy Particles*, New-York, 1952

[10] U.Seddik, P.Moskal, *Performance of Amadeus and S1 for Identification of Two Particles with Small Relative Distance*, Report KFA-IKP(1), 1996

[11] S.Brauksiepe, *Die Effizienz des Zwei-Protonen-Triggers am internen Experiment COSY-11*, KFA IKP,Jülich-3202, 1996